Extending the Validation of Multi-Mode Model for Anomalous Transport to High Beta Poloidal Tokamak Scenario in DIII-D

A.Y. Pankin[a],[1] A.H. Kritz,[2] T. Rafiq,[2] A.M. Garofalo,[3] I. Holod,[1] and J. Weiland[4]

[1]*Lawrence Livermore National Laboratory, Livermore, CA 94550, USA*

[2]*Lehigh University, Bethlehem, CA 18015, USA*

[3]*General Atomics, San Diego, CA 92121, USA*

[4]*Chalmers University of Technology,*

SE-412 96 Göteborg, Sweden; Euratom-VR Association

(Dated: March 1, 2018)

[a] Current affiliation: Lehigh University, Bethlehem, PA 18015

Abstract

The Multi-Mode Model (MMM7.1) for anomalous transport is tested in predictive modeling of temperature profiles of a high beta poloidal DIII-D discharge. This new H-mode plasma regime, with high beta poloidal and high bootstrap currents, has been studied in DIII-D tokamak discharges [A. Garofalo *et al.* Nuclear Fusion 55, 123025 (2015)]. The role of turbulent modes described by MMM7.1 is investigated. The temperature profiles for a high beta poloidal DIII-D discharge are computed using the NCLASS model for the neoclassical transport and the Weiland and ETG components of the MMM7.1 model for the anomalous transport. The neoclassical transport is found to be the main contributor to the ion thermal transport in the plasma core. The contributions from the ion temperature gradient driven modes are found to be important only outside of the internal transport barrier. The magnitudes of the predicted temperature profiles are found to be in a reasonable agreement with experimental profiles. The simulation results approximately reproduce the internal transport barrier in ion temperature profile, but not in the electron temperature profile due to a weak dependence of the ETG driven transport on the Shafranov shift in the ETG component of MMM7.1. Possible effects that can contribute to stabilization of these modes, for example, effects associated with the large beta poloidal such as the Shafranov shift stabilization in the MMM7.1 model, are discussed. It is demonstrated that the $\mathbf{E} \times \mathbf{B}$ flow shear plays a relatively small effect in the formation of the internal transport barrier in the high beta poloidal DIII-D discharge 154406. The Shafranov shift (alpha stabilization) and small or reversed magnetic shear profiles are found to be the primary reasons for quenched anomalous transport in this discharge.

I. INTRODUCTION

The importance of reliable predictions of plasma profiles is related to the development of new operational tokamak scenarios and to the prediction of plasma performance in future tokamaks such as ITER. A robust and reliable model for anomalous transport is also important for real-time control techniques and for understanding the role of various transport mechanisms in tomakak plasmas. Independent of the fidelity level, each model has its range of applicability. The theoretical assumptions that are utilized in the model development provide some guidance for the ranges of model applicability. However, the ultimate test for model applicability ranges can provide only a careful validation of model results in different plasma parameter regimes.

In this research, the Multi-Mode Model (MMM7.1) for anomalous transport [1] is tested in predictive modeling of temperature profiles of a high beta poloidal discharge in DIII-D. The Multi-Mode Model has been previously validated in the most conventional plasma regimes including the Ohmic, low- and high- confinement modes [2, 3]. A new H-mode plasma regime with high beta poloidal and high plasma currents has been recently studied in the DIII-D and EAST tokamaks [4–7]. This regime is characterized by a high bootstrap current fraction and a steady-state operation. Typically, these discharges have internal transport barriers at large radius and with $\beta_p, \beta_N > 3$. Previously, the MMM7.1 model has not been tested for discharge scenarios of this type and this paper reports first validation results of the MMM7.1 model for high beta poloidal DIII-D discharges.

The experimental findings for a fully noninductive, high beta poloidal DIII-D discharge 154406 that is analyzed here have been previously reported in Ref. [4]. The surface voltage remains at near zero values for most of the duration of the discharge after the flat top is established at the level of 0.6 MA. The values of β_N and β_p exceed 3, and β_T remains around 1.5 % during the fully noninductive stage of the discharge. The auxiliary heating power and current drive consist of 8.5 MW of neutral beam injection (NBI) and 2.5 MW of electron cyclotron current drive (ECCD). The ECCD and 5 MW of the NBI power are applied off-axis. Good confinement has been achieved in this discharge with $H_{98\mathrm{y},2} > 1$. The improved confinement has been related to the formation of a transport barrier at $r/a \approx 0.7$ as shown in Ref. [4].

Analysis of high-beta poloidal DIII-D experiments using the TGLF module [8] showed that the saturated turbulence levels for ETG driven modes need to be artificially increased in order to reproduce experimental profiles [7]. In this study, it is demonstrated that the drift resistive inertial ballooning model which is a part of MMM7.1 does not perform well for these discharges due to the lack of the Shafranov shift stabilization effect in the model. It is also demonstrated that the Weiland component of MMM7.1 produces too much transport in the regions of electron ITB. The ion ITB is reproduced more reliably as well as the electron and ion temperatures in the region near the magnetic axis with the normalized minor radius $r/a<0.3$. The effects of the $\mathbf{E}\times\mathbf{B}$ flow shear and Shafranov shift on the anomalous transport are investigated.

The remainder of this paper is organized as follows. Sec. II describes the modeling framework. In Sec. III, the results from different components of MMM7.1 are presented and compared to the experimental observations. The comparison of the $\mathbf{E} \times \mathbf{B}$ flow shear to the Shafranov shift effects is discussed. Finally, summary of the modeling carried out are discussed and possible future research directions are described.

II. MODELING FRAMEWORK

The PTRANSP code, which is the TRANSP analysis code [9] extended for use in carrying out predictive integrated modeling simulations, is used in this research. The PTRANSP code is designed to predict the evolution of temperature, density and toroidal velocity profiles. It includes a choice of anomalous and neoclassical transport models, models for sources and various equilibrium solvers. In this study, the Multi-Mode Model (MMM7.1) [1] is used to predict the evolution of electron and ion temperature profiles. The NCLASS model [10] is used to compute the neoclassical transport. The power deposition and current driven profiles associated with neutral beam injection is computed using the NUBEAM module [11]. The deposition profiles associated with the electron cyclotron current drive (ECCD) are computed using the TORAY module [12].

The anomalous transport driven by the drift-wave turbulence is usually very sensitive to the safety factor profiles. In this study of anomalous transport in a high beta poloidal discharge, the equilibrium has not been evolved in a predictive manner in order to keep the focus of this research on the validation of transport models. Instead, the time dependant experimental equilibrium reconstruction with the EFIT code [13] is used.

A. Multi-Mode Model (MMM7.1) for anomalous transport

The MMM7.1 consists of a combination of contributions from different transport theories. It includes the Weiland module for ion temperature gradient modes, trapped electron modes and collision dominated MHD modes [14], the Rafiq module for drift-resistive-inertial ballooning modes (DRIBM) [15], paleoclassical transport model [16], and the Horton module with the Jenko threshold [17] for anomalous transport driven by Electron Temperature Gradient (ETG) modes. The Weiland and DRIBM components of MMM7.1 are based on the linearized fluid equations with magnetic drift for each particle species.

The MMM7.1 model has been installed and used in the PTRANSP code. There is an option to enable or disable individual components of MMM7.1 in PTRANSP in order to test the contribution from different transport mechanisms in different regions of tokamak discharges and in different plasma regimes. In particular, it is known that the Weiland and Horton components mostly contribute to the transport in the plasma core, while the paleoclassical and DRIBM components mostly contribute in the plasma edge region with the normalized minor radii r/a>0.8. In addition, the drift-resistive inertial ballooning modes are stabilized with increasing temperature and the DRIBM model yields significantly larger contributions to the thermal and particle transport in the low-confinement (L-mode) discharges than in the high-confinement (H-mode) discharges [3]. In this research, the anomalous transport in the plasma core region of the H-mode discharge is investigated. The boundary conditions are set at r/a=0.8 and the DRIBM and paleoclassical models are not considered in this study.

The Weiland component includes the electromagnetic and finite β effects, electron-ion collisions, trapped electrons, impurities, and fast ions. In the Weiland component, the growth rates, frequencies and eigenfunctions are computed from a system of nine perturbed fluid equations with drifts. The particle, thermal, and momentum fluxes in the model are computed for the fastest growing ion and electron modes. The diffusion matrix is computed as a derivative of the heat, particle and momentum fluxes, obtained in a quasilinear approximation. The model can be used for the computation of thermal and particle transport as well as for the computation of toroidal and poloidal angular momentum transport. At this time, not all transport mechanisms are completely implemented in the PTRANSP transport solvers and the focus of this research will remain on the investigation of thermal transport.

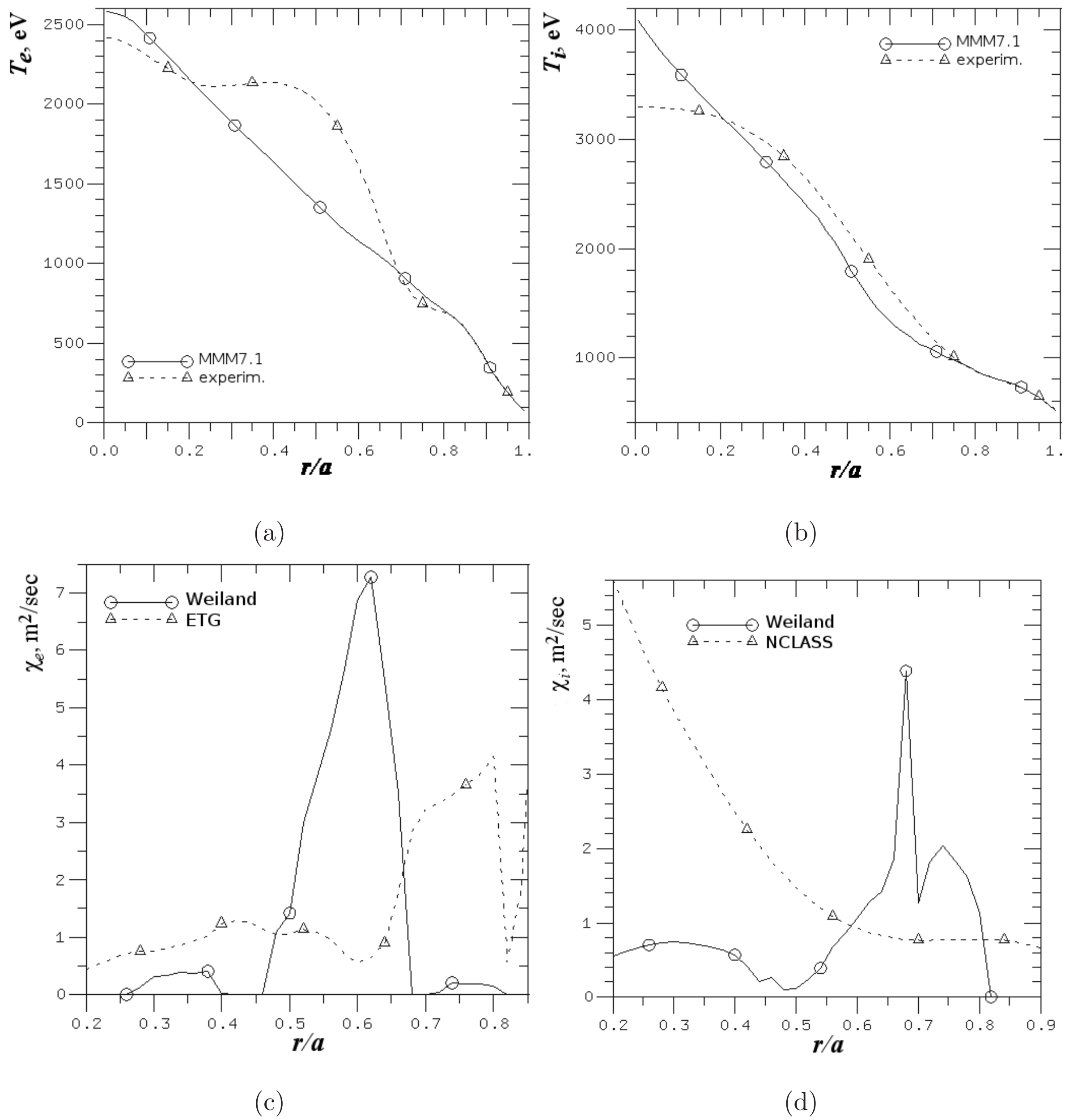

FIG. 1. Results of predictive modeling of high beta poloidal DIII-D discharge 154406 at 5.2 seconds using the Weiland and ETG components of MMM7.1. The predicted electron (a) and ion (b) temperature profiles are compared to the experimental profiles. The effective electron thermal diffusivities from the Weiland (solid curve) and ETG (dashed curve) components of MMM7.1 are shown in panel (c). The effective ion thermal diffusivities from the Weiland model (solid curve) and neoclassical thermal diffusivities from the NCLASS model (dashed curve) are shown in panel (d).

III. PREDICTIVE MODELING RESULTS

A. Instabilities that drive the anomalous transport in high beta poloidal discharges

The role of different modes described by MMM7.1 is investigated in this research. In particular, the temperature profiles for the high beta poloidal DIII-D discharge 154406 are predicted using the Weiland and ETG components of MMM7.1. The predicted temperature profiles are compared to the corresponding temperature profiles from the interpretive TRANSP simulations. Fig. 1 shows the predicted electron and ion temperature profiles for the DIII-D discharge 154406. Reasonable agreement between predicted and experimental ion temperature profiles is observed. The predicted electron and ion temperatures in the plasma core are close to the experimental values. However, the electron temperature profile does not have an ITB and the location of ITB in the ion temperature profile can not be accurately reproduced in the predictive MMM7.1 simulations. The reason is a rather significant electron thermal transport from the ETG components of MMM7.1 that prevents an ITB from forming in the electron temperature profile (see Fig. 1c). The role of ETG driven transport computed with the ETG model in MMM7.1 is found to be very different from the simulations with TGLF model [7, 18]. In contrast to the MMM7.1 model, TGLF predicts a very strong ITB in the electron temperature profiles. However, the level of ETG transport in the simulations with the TGLF model is found to be too low. The experimental electron and ion temperature profiles can be reproduced only with an artificial multiplier for the ETG transport [7]. Most likely the reason for the deficiency of the ETG model in MMM7.1 is related to the fact that the model does not have a strong dependence on the Shafranov shift. The parametric dependence on the Shafranov shift for the ETG driven transport can be improved through a serious of systematic scans with a gyro-kinetic code, and by reintroducing the Shafranov dependence back to the ETG model in MMM7.1. This work will be a part of future studies. Comparing the predicted and experimental ion temperature profiles in Fig. 1b one can also notice that the predicted ion temperature exceeds the experimental ion temperature near the magnetic axis by approximately 20%, which might be related to some unstable interchange modes that are not described by the Weiland component.

The ion thermal anomalous and neoclassical diffusivities are compared in Fig. 1d. The

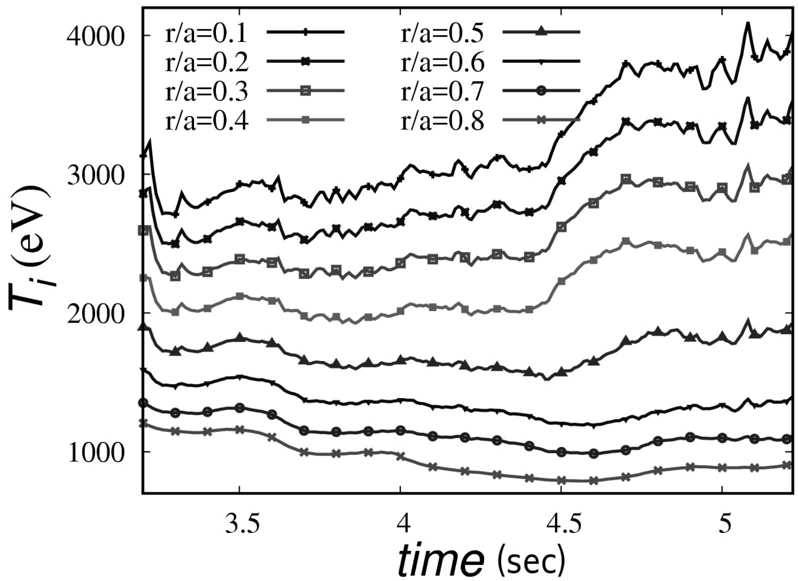

FIG. 2. Ion temperatures at different radial location as functions of time in the PTRANSP simulations.

ion anomalous transport exceeds the neoclassical transport level only in the vicinity region of ITB. The time trace of the ion temperature at different radial location in Fig. 2 shows the formation of the internal transport barrier at 4.5 sec between r/a of 0.4 and 0.6. The predicted time of ITB formation agrees with the ITB formation time in experiment. At this time, both β_p and β_N reach maximum values in this experiment above 3 (see Fig. 1 in Ref. [4]).

It should be noted that the peak contribution from the Weiland component significantly exceeds the contribution from the ETG component. The contour plot of maximum growth rates computed with the Weiland component are shown in Fig. 3 as a function of time and normalized minor radius. The area of reduced growth rates is forming at approximately 4.5 seconds, which agrees with the ion temperature dynamics shown in Fig. 2. The growth rates are also found to be significantly lower in the ITB region. This is consistent with the reduced ion transport inside of ITB.

B. Role of the $\mathbf{E}\times\mathbf{B}$ flow shear and Shafranov shift effects

It is important to separate the effects associated with the $\mathbf{E}\times\mathbf{B}$ flow and Shafranov shifts on the anomalous transport in order to improve the predictive capabilities of the integrated

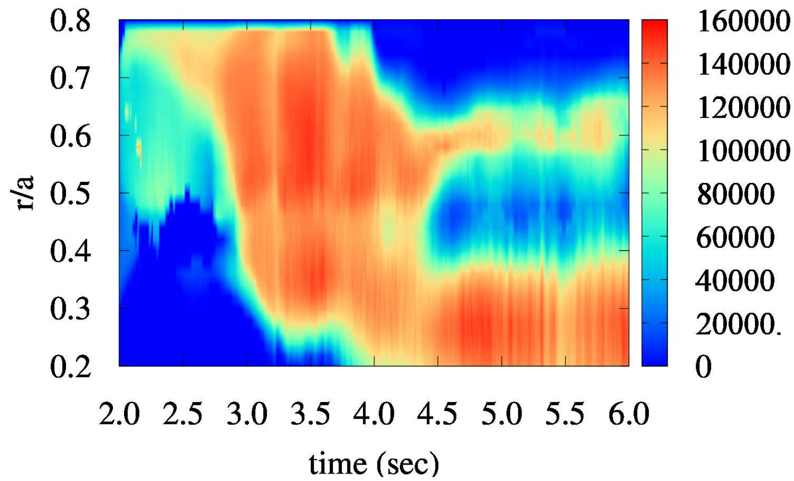

FIG. 3. Maximum growth rates predicted using the Weiland component of MMM7.1 and shown as color map in 1/sec as a function of time and radial location in the PTRANSP simulations for the DIII-D discharge 154406.

modeling of high beta poloidal discharhges. In the Weiland component of MMM7.1, the $\mathbf{E} \times \mathbf{B}$ flow shear effect is included by subtracting the $\mathbf{E} \times \mathbf{B}$ flow shear rates from the growth rates of the most unstable models. The high beta poloidal DIII-D discharge 154406 has a relatively low torque and the effect from the ExB flow shear is expected to be small. This hypothesis can be confirmed by the results of the predictive modeling of temperature profiles with different toroidal velocity profiles. Fig. 4 shows that the predicted electron and ion temperature profiles with and without the $\mathbf{E} \times \mathbf{B}$ flow shear effect are almost coincide, confirming that the effect from the $\mathbf{E} \times \mathbf{B}$ flow shear on the anomalous transport is very weak in this discharge. The differences in the temperature profile predictions become notable for the toroidal velocity profiles scaled by the factor of 5. The temperature profiles predicted with the experimental toroidal velocity profiles scaled by the factor of 10 are shown in Fig. 4 as solid curves. The $\mathbf{E} \times \mathbf{B}$ flow shear effect is affecting mostly the ion temperature profiles because the ETG modes that significantly contribute to the electron thermal transport are not affected by the $\mathbf{E} \times \mathbf{B}$ flow shear in MMM7.1.

The Shafranov shift effect is included in the Weiland component of MMM7.1 through a geometric factor in the expression for the ion drift magnetic frequency:

$$\omega_{Dj} = \frac{-2k_\theta T_j}{Z_j eBR}\left(\cos\theta + s\theta\sin\theta + \alpha_m \sin^2\theta\right),$$

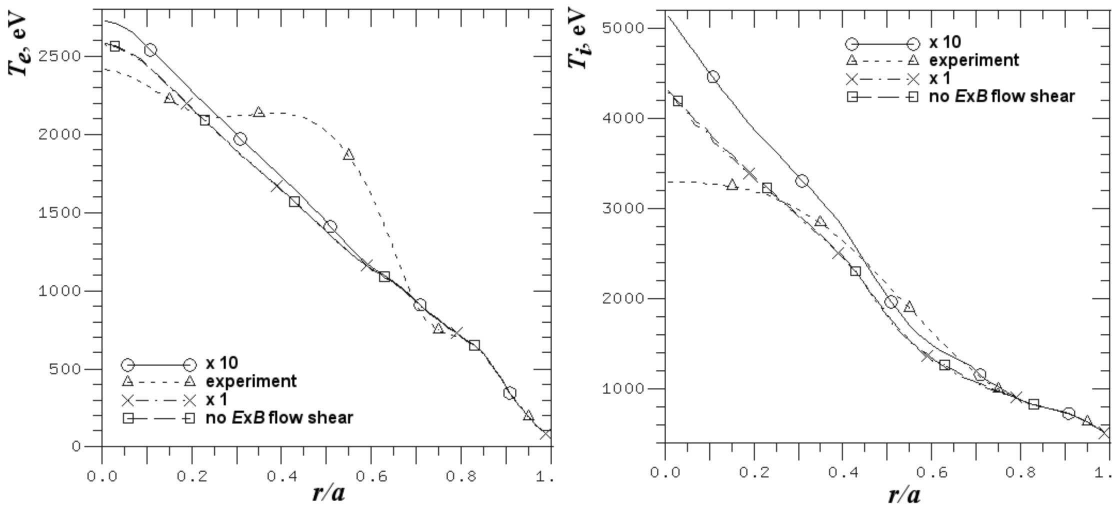

(a) (b)

FIG. 4. Electron (a) and ion (b) temperature profiles as functions of normalized minor radius for different toroidal velocity profiles. The profiles predicted without $\mathbf{E}\times\mathbf{B}$ effect are shown as long dashed lines. The profiles predicted without the $\mathbf{E}\times\mathbf{B}$ effect are shown as long-dashed curves. The predicted temperature profiles with the experimental toroidal velocity profile are shown as dash-dotted curves. The temperature profiles predicted with the toroidal velocity profiles scaled by factor of 10 are shown as solid curves. The predicted profiles are compared to the experimental temperature profiles shown as short dashed curves.

where j is the ion species index, Z is the ion charge, k_θ is the wave vector in the poloidal direction, s is the magnetic shear, θ is the poloidal angle, and α_m is the alpha MHD defined as $\alpha_m = \frac{2\mu_0 R q^2}{B^2}\frac{dp}{dr}$. Here, p is the plasma pressure, R is the major radius and q is the safety factor.

The Shafranov shift scan is done by introducing a scaling factor C_{ss} for α_m, which is proportional to the Shafranov shift:

$$\omega_{Dj} = \frac{-2k_\theta T_j}{Z_j e B R}\left(\cos\theta + s\theta\sin\theta + C_{ss}\alpha_m \sin^2\theta\right).$$

The thermal diffusivities and temperature profiles predicted for the different values of the coefficient C_{ss} are shown in Fig. 5. The ion thermal diffusivities are reduced with the increased coefficient C_{ss} for all radial locations. The electron thermal diffusivities are reduced with the increased coefficient C_{ss} for r/a<0.55, but are weakly affected in the region of electron ITB. As a result of the reduced ion and electron thermal transport, the ion and

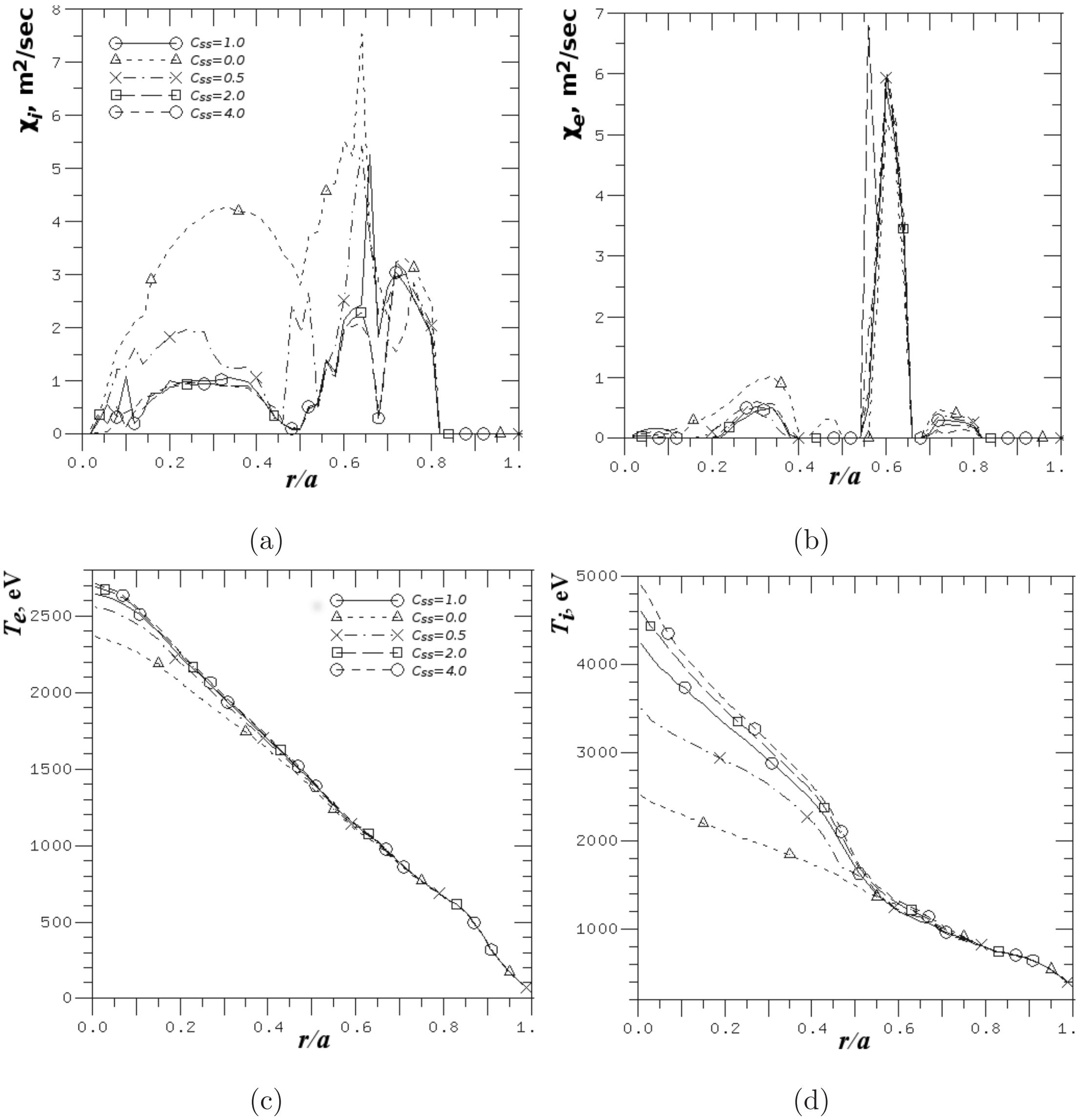

FIG. 5. Ion (a) and electron (b) thermal diffusivities profiles and electron (c) and ion (d) temperature profiles as functions of the normalized minor radius for different values of the coefficient C_{ss} that represent the Shafranov shift effect.

electron temperatures increase with the increased coefficient C_{ss} as seen in Fig. 5c and 5d. The effect on the ion temperature profile is found to be much stronger than the effect on the electron temperature profile, which might be related to an electron mode that is weakly affected by the Shafranov shift. The Shafranov shift stabilization effect for the values above experimental relevant values is found to be relatively weak. The ion ITB disappears for the values of C_{ss}<0.5.

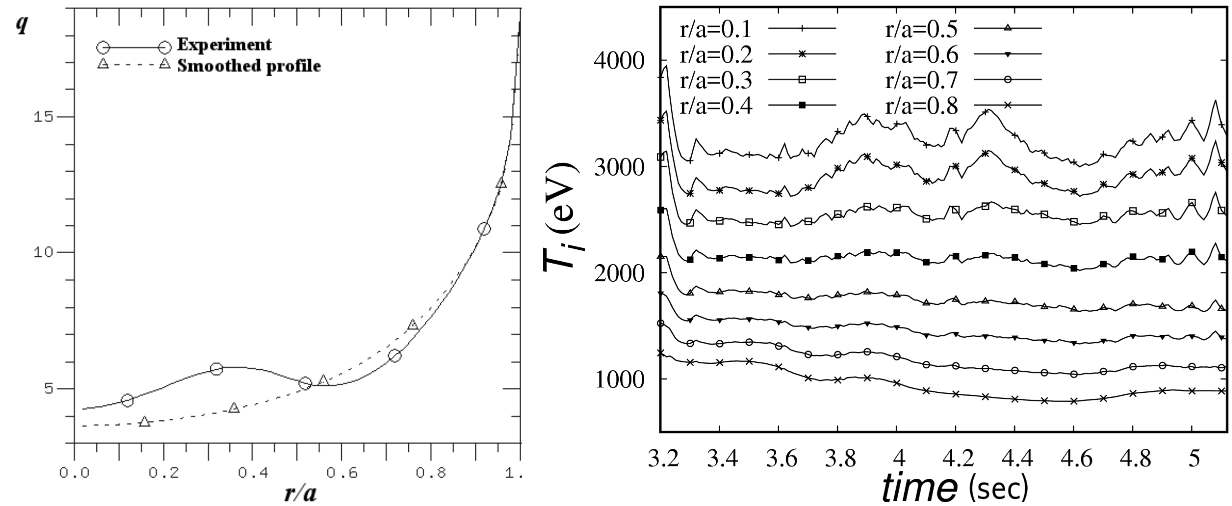

(a) (b)

FIG. 6. (a) The q-profiles as functions of normalized minor radius at 5.1 sec based on the equilibrium reconstruction (solid curve) and smoother over radius; (b) The ion temperatures at different radial locations as functions of time for smoothed q-profile.

C. The effect of q-profile on the formation of internal transport barrier

In the DIII-D experiments, the formation of internal transport barriers in the high beta poloidal discharge is found to depend on the q-profiles [6]. In particular, it is reported that "a small range of local q profile or magnetic shear is favorable for the better confinement due to the observation of appearance and disappearance of strong ITB during the plasma current ramp-up phase". The dependence of the ITB formation on the magnetic shear is also investigated using the predictive PTRANSP simulations with the MMM7.1 model. In these simulations, the experimental q-profiles are smoothed so that there is no local minimum around $r/a = 0.6$ where the parallel current density is peaked. While all other parameters remain the same, the simulation with the smoothed q-profile does not show the formation on internal transport barrier as it shown in Fig. 6. The ion temperatures in the plasma core are significantly lower than the core ion temperatures shown in Fig. 2 that are produced in the simulation that utilized the q-profiles derived from the experimental equilibrium reconstruction. This simulation confirms that the small or reversed magnetic shear along with the Shafranov shift plays an important role in the triggering of internal transport barrier in high beta poloidal DIII-D discharges.

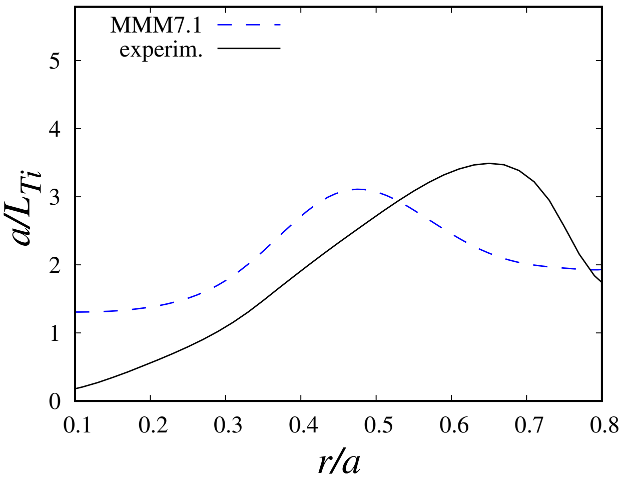

FIG. 7. Smoothed normalized gradients of predicted and experimental ion temperature profiles as functions of normalized minor radius.

IV. SUMMARY

In this research, the high beta poloidal DIII-D discharge 154406 is investigated using the components of MMM7.1 model. In the simulations with the Weiland and ETG components of MMM7.1, the boundary conditions have been set at $r/a = 0.8$. A reasonable agreement between the simulation results and experimental data is obtained for the ion temperature profiles in the plasma core with the exception of the area in a close proximity to the magnetic axis. In this region, the ion temperature is found approximately 20% higher than the experimental values. The internal transport barrier for the ion temperature profile is reproduced. However, there is some disagreement in the ITB foot location. The difference in the ITB foot location can be also easily seen in Fig. 7 that compares the gradients of predicted and experimental ion temperature profiles. The predicted ITB foot location is shifted more towards the plasma core compared to the ITB foot location in the experimental ion temperature profile. The predicted electron temperature at the magnetic axis is close to the experimental values. However, due to a weak dependence of the ETG driven transport on the Shafranov shift in the ETG model in MMM7.1, an ITB in the electron temperature profile is not correctly reproduced. The dependence of ETG driven transport needs to be improved. This work will be a part of future studies.

It is demonstrated that the neoclassical transport is the main transport channel for the ion temperature profiles in the plasma core. The contributions to the electron thermal transport from ITG and ETG modes are important for the prediction of electron temperature profiles. The contribution from the ETG model is found to be important across the whole radius, and the electromagnetic effects on the ETG modes are found to be important from approximately $r/a \approx 0.6$. The anomalous ion thermal transport is mostly driven by the ITG modes. The ion neoclassical thermal transport exceeds the anomalous transport for the most of profiles except outside the ITB region, where the ITG driven transport is significantly larger than the neoclassical transport.

The effects of $\mathbf{E} \times \mathbf{B}$ flow shear and Shafranov shift are compared. It is shown that the $\mathbf{E} \times \mathbf{B}$ flow shear has a small effect on the anomalous transport in this DIII-D discharge. Due to a small role of the $\mathbf{E} \times \mathbf{B}$ flow shear, the high beta poloidal discharge scenario can be very promising for achieving an improved core confinement with a reduced NBI torque. Stabilization effect from the Shafranov shift is found to be dominating for the ion channel. It is also found that the small or reversed magnetic shear contributes to the formation of internal transport barrier in the high beta poloidal DIII-D discharge 154406. The experimental values of Shafranov shift are found to yield the effect that is close to the maximum possible stabilization due to the Shafranov shift stabilization. The combination of the this effect and small magnetic shear is found to be essential for the formation of the ion ITB and improved confinement in the high beta poloidal DIII-D discharges.

ACKNOWLEDGEMENTS

This work was performed under the auspices of the U.S. Department of Energy by Lawrence Livermore National Laboratory under Contract No. DE-AC52-07NA27344. This work is also supported by the U.S. Department of Energy, Office of Science, under Award Numbers DE-SC0012174 and DE-FC02-04ER54698. The authors would like to thank the TRANSP code developers especially Dr. X. Yuan for his help with updates of diagnostic output from anomalous transport models inside TRANSP.

[1] T. Rafiq, A. Kritz, J. Weiland, A. Pankin, and L. Luo, Phys. Plasmas **20**, 032506 (2013).

[2] V. Genty, T. Rafiq, A. Kritz, and A. Pankin, in *Proc. 54th Annual Meeting of the APS Division of Plasma Physics ((Providence, RI, October 29-November 2, 2012)*, Vol. 57 (2012)

p. JP8.00020.

[3] T. Rafiq, A. Kritz, V. Tangri, A. Pankin, I. Voitsekhovitch, and R. Budny, Phys. Plasmas **21**, 122505 (2014).

[4] A. Garofalo, X. Gong, B. Grierson, Q. Ren, W. Solomon, E. Strait, M. V. Zeeland, C. Holcomb, O. Meneghini, S. Smith, G. Staebler, B. Wan, R. Bravenec, R. Budny, S. Ding, J. Hanson, W. Heidbrink, L. Lao, G. Li, C. Pan, C. Petty, J. Qian, C. Paz-Soldan, and G. Xu, Nuclear Fusion **55**, 123025 (2015).

[5] X. Gong, B. Wan, J. Li, and A. M. Garofalo, in *Proceedings of 25th IAEA Fusion Energy Conference (Saint Petersburg, Russia, 13-18 October 2014)* (2014) pp. EX/P2–39.

[6] S. Ding, G. Xu, Q. Wang, W. Solomon, Y. Zhao, X. Gong, A. Garofalo, C. Holcomb, G. McKee, Z. Yan, H. Wang, J. Qian, and B. Wan, Nuclear Fusion **57**, 022016 (2017).

[7] C. Pan, G. Staebler, L. Lao, A. Garofalo, X. Gong, Q. Ren, J. McClenaghan, G. Li, S. Ding, J. Qian, B. Wan, G. S. Xu, W. Solomon, O. Meneghini, and S. Smith, Nuclear Fusion **57**, 036018 (2017).

[8] G. Staebler, J. Kinsey, and R. Waltz, Phys. Plasmas **12**, 102508 (2005).

[9] J. Ongena, M. Evrard, and D. McCune, Transactions of Fusion Technology , 181 (1998).

[10] W. Houlberg, K. Shaing, S. Hirshman, and M. Zarnstorff, Phys. Plasmas **4**, 3230 (1997).

[11] A. Pankin, D. McCune, R. Andre, G. Bateman, and A. Kritz, Computer Physics Communications **159**, 157 (2004).

[12] A. Kritz, H. Husan, R. Goldfinger, and D. Batchelor, in *Proc. 3rd Joint Varenna-Grenoble Inf. Symposium on Heating in Toroidal Plasma. Brussels: Commission of the European Communities*, Vol. 11 (1982) p. 707.

[13] L. Lao, H. S. John, R. Stambaugh, A. Kellman, and W. Pfeiffer, Nuclear Fusion **25**, 1611 (1985).

[14] J. Weiland, *Stability and Transport in Magnetic Confinement Systems* (Springer, 2012).

[15] T. Rafiq, G. Bateman, A. Kritz, and A. Pankin, Phys. Plasmas **17**, 082511 (2010).

[16] J. Callen, Nucl. Fusion **45**, 1120 (2005).

[17] G. Bateman, A. H. Kritz, A. Y. Pankin, T. Onjun, J. E. McElhenny, and C. MacDonald, Plasma Physics and Controlled Fusion **48**, A93 (2006).

[18] J. McClenaghan, A. Garofalo, O. Meneghini, S. Smith, J. Leuer, G. Staebler, L. Lao, J. Park, S. Ding, X. Gong, and J. Qian, Nuclear Fusion **57**, 116019 (2017).